Available online at www.sciencedirect.com
SCIENCE DIRECT®
Journal of Computational Physics 198 (2004) 389–402
JOURNAL OF COMPUTATIONAL PHYSICS
www.elsevier.com/locate/jcp

Short Note

A convexity preserving scheme for conservative advection transport

Feng Xiao [a,*], Xindong Peng [b]

[a] Department of Energy Sciences, Tokyo Institute of Technology, 4259 Nagatsuta, Midori-ku, Yokohama 226-8502, Japan
[b] Earth Simulator Center, JAMSTEC, 31731-25, Showamachi, Kanazawa-ku, Yokohama 236-0001, Japan

Received 17 November 2003; received in revised form 15 January 2004; accepted 20 January 2004
Available online 20 February 2004

Abstract

A simple and practical scheme for advection transport equation is presented. The scheme, namely piecewise rational method (PRM), is a variant of the existing piecewise parabolic method (PPM) of Colella and Woodward (1984). Instead of the parabolic function, a rational function is used for the reconstruction. Making use of the convexity preserving nature of the rational function enables us to obtain oscillation-less numerical solutions, but avoids the adjustments of the cell-interface values to enforce the monotonicity in PPM. The PRM is very simple and computationally efficient. Our numerical results show that PRM is competitive to the PPM in many aspects, such as numerical accuracy and shape-preserving property.

AMS: 65C20; 76M20; 76T05; 65P05; 77F05

Keywords: Advection transport; Computational algorithm; Rational interpolation; Convexity preserving; Numerical oscillation; Mass conservation

1. Introduction

A class of conservative schemes for the advection equation has been so far proposed following the pioneering work of Godunov [5]. A Godunov type scheme computes the cell-integrated average values of a prognostic variable by using a conservative finite difference method of flux form, or a finite volume method as preferred by some researchers, and results in an exact conservation for the transported quantity. High order Godunov schemes can be devised by reconstructing high order interpolations within each mesh cell. Rather than the piecewise constant interpolation in the original Godunov scheme, a linear interpolation

* Corresponding author. Tel./fax: +81-45-924-5538.
E-mail address: xiao@es.titech.ac.jp (F. Xiao).

0021-9991/$ - see front matter © 2004 Elsevier Inc. All rights reserved.
doi:10.1016/j.jcp.2004.01.013

function and a parabolic polynomial were used in the MUSCL [11,12] and the piecewise parabolic method (PPM) [4] schemes. Among the high resolution schemes, the MUSCL and the PPM have so far shared a large popularity in various applications.

Basically, using a linear or higher order interpolation function for reconstruction tends to bring about oscillations to the numerical solutions. To get rid of this, slope modifications and the adjustments of the cell-interface values prove to be necessary. As a result, the piece-wisely constructed interpolation function is not usually continuous cross the cell interfaces. This short note presents a variant to the existing PPM by making use of a rational interpolation function. The resulting scheme, which is called piecewise rational method (PRM), makes use of a rational function to reconstruct the sub-cell interpolation. Due to the convexity preserving property of the rational function, the PRM scheme gives an oscillation-less solution but does not need the adjustments for the cell-interface values. The performance of PRM is evaluated in this note by numerical experiments.

The interpolation functions and the numerical formulation of PRM are described in Sections 2 and 3. Numerical experiments with comparisons with the PPM scheme are given in Section 4. The paper is ended with a few conclusion remarks in Section 5.

2. The interpolation reconstruction

Constructing a high order Godunov scheme begins with the reconstruction of the sub-cell interpolation function from the given cell-average values for all computational cells. Provided a physical variable $f(x)$ is discretized over a 1D grid partition with each cell defined by $[x_{i-\frac{1}{2}}, x_{i+\frac{1}{2}}]$ for $i = 0, 1, \ldots, i_{\max}$, the cell-average of $f(x)$ is computed by

$$\bar{f}_i = \frac{1}{\Delta x_i} \int_{x_{i-\frac{1}{2}}}^{x_{i+\frac{1}{2}}} F_i(x)\mathrm{d}x, \tag{1}$$

with $\Delta x_i = x_{i+\frac{1}{2}} - x_{i-\frac{1}{2}}$, and $F_i(x)$ being the piecewise interpolation function.

Given the cell-integrated averages $\bar{f}_i$ and the cell interface values $f_{i-\frac{1}{2}}$ and $f_{i+\frac{1}{2}}$, an interpolation function with a freedom of three can be constructed over the ith cell $[x_{i-\frac{1}{2}}, x_{i+\frac{1}{2}}]$. The cell-interface values, $f^n_{i-\frac{1}{2}}$ for $i = 0, 1, \ldots, i_{\max}$, can be determined by either making use of an interpolation approximation based on the known cell-average values or treating the interface value as another prognostic variable which is memorized and advanced at every time step. The latter results in a class of advection transport schemes called CIP-CSL schemes [13,15,16]. In this brief note, we take the conventional way and compute the cell interface values by an interpolation approximation which is only based on the cell average values. Being an example of such a kind, a cubic polynomial can be derived from 4 cell averages and the resulting interpolated value at $x_{i+\frac{1}{2}}$ is

$$f_{i+\frac{1}{2}} = \tfrac{7}{12}(\bar{f}_i + \bar{f}_{i+1}) - \tfrac{1}{12}(\bar{f}_{i-1} + \bar{f}_{i+2}) \tag{2}$$

for a uniform grid.

It is well-known that any high order interpolation tends to create spurious oscillations in numerical solutions. As a remedy for this, slope modifications were introduced in the MUSCL [11,12] and the PPM [4] schemes. In this paper, we adopted the method of Colella and Woodward [4] for computing the interface values as,

$$f_{i+\frac{1}{2}} = \tfrac{1}{2}(\bar{f}_i + \bar{f}_{i+1}) - \tfrac{1}{6}(\bar{\delta} f_i - \bar{\delta} f_{i-1}), \tag{3}$$

with $\bar{\delta} f_i$ being the average slope in cell $[x_{i-\frac{1}{2}}, x_{i+\frac{1}{2}}]$ (see [4] for the expression over a non-uniform mesh). The following approximation formula for the average slope was intensively discussed and used in the MUSCL and the PPM schemes,

$$\bar{\delta} f_i = \begin{cases} \min(|\delta f_i|, \alpha_1|\bar{f}_{i+1} - \bar{f}_i|, \alpha_2|\bar{f}_i - \bar{f}_{i-1}|)\mathrm{sgn}(\delta f_i), & \text{if } (\bar{f}_{i+1} - \bar{f}_i)(\bar{f}_i - \bar{f}_{i-1}) > 0, \\ 0, & \text{otherwise}, \end{cases} \tag{4}$$

where $\delta f_i = (\bar{f}_{i+1} - \bar{f}_{i-1})/2$. The positives α_1 and α_2 are parameters that control the average slope and affect the dispersion errors of the numerical solutions. For the rational function based scheme discussed in this note, we used $\alpha_1 = \alpha_2 = 3$.

With $\bar{f}_i$, $f_{i-\frac{1}{2}}$ and $f_{i+\frac{1}{2}}$ known, we can uniquely construct the piecewise interpolation function $F_i(x)$ by using the following constraint conditions

$$F_i(x_{i-\frac{1}{2}}) = f_{i-\frac{1}{2}}, \tag{5}$$

$$F_i(x_{i+\frac{1}{2}}) = f_{i+\frac{1}{2}}, \tag{6}$$

$$\frac{1}{\Delta x_i} \int_{x_{i-\frac{1}{2}}}^{x_{i+\frac{1}{2}}} F_i(x)\mathrm{d}x = \bar{f}_i. \tag{7}$$

A parabolic function, as used in the PPM scheme, can be defined as

$$F_i(x) \equiv P_i(x) = a_i + b_i(x - x_{i-\frac{1}{2}}) + c_i(x - x_{i-\frac{1}{2}})^2 \quad \text{for } x \in [x_{i-\frac{1}{2}}, x_{i+\frac{1}{2}}]. \tag{8}$$

The interpolated profiles for a triangular pulse and a step jump are plotted in Fig. 1, the parabolic function has produced significant overshots and undershots near the large gradients, which then appear as the spurious oscillations in the numerical solutions. In order to get rid of the numerical oscillations, the PPM scheme re-adjusts the interface value $f_{i+\frac{1}{2}}$ into $f_{Li+\frac{1}{2}}$ and $f_{Ri+\frac{1}{2}}$ for the use of two neighboring cells (consult [4] for the details). The adjustment procedure for monotonicity is clearly illustrated in [2] (see Figs. 3–5 of [2] and the related discussions). A discontinuity or jump often occurs between $f_{Li+\frac{1}{2}}$ and $f_{Ri+\frac{1}{2}}$, especially in the vicinity of large gradient.

Instead of (8), we use a rational function in a form as,

$$F_i(x) \equiv R_i(x) = \frac{a_i + 2b_i(x - x_{i-\frac{1}{2}}) + \beta_i b_i (x - x_{i-\frac{1}{2}})^2}{[1 + \beta_i(x - x_{i-\frac{1}{2}})]^2} \quad \text{for } x \in [x_{i-\frac{1}{2}}, x_{i+\frac{1}{2}}]. \tag{9}$$

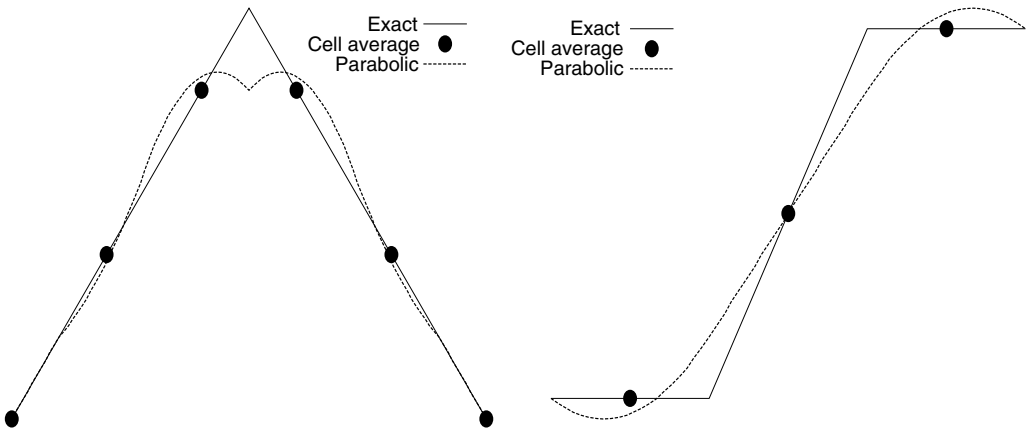

Fig. 1. Reconstruction for a triangle peak (left) and a step jump (right) by a parabolic function.

From (5)–(7), the rational function (9) can be uniquely determined, and the coefficients read

$$a_i = f_{i-\frac{1}{2}}, \tag{10}$$

$$b_i = \beta_i \bar{f}_i + \frac{1}{\Delta x_i}(\bar{f}_i - f_{i-\frac{1}{2}}), \tag{11}$$

$$\beta_i = \Delta x_i^{-1}\left[\frac{(f_{i-\frac{1}{2}} - \bar{f}_i)}{(\bar{f}_i - f_{i+\frac{1}{2}})} - 1\right]. \tag{12}$$

Note that in case of $(\bar{f}_i - f_{i+\frac{1}{2}})(f_{i-\frac{1}{2}} - \bar{f}_i) < 0$, singularity may arise when $1 + \beta_i(x - x_{i-\frac{1}{2}})$ approaches 0. This is the case where a peak or a ravine is transported. A simple remedy can be devised by modifying β_i into

$$\tilde{\beta}_i = \Delta x_i^{-1}\left[\frac{|f_{i-\frac{1}{2}} - \bar{f}_i| + \epsilon}{|\bar{f}_i - f_{i+\frac{1}{2}}| + \epsilon} - 1\right], \tag{13}$$

with ϵ being a small positive to avoid division by zero when $\bar{f}_i - f_{i+\frac{1}{2}} = 0$. The small number ϵ serves only to avoid division by zero, thus it can be set as small as machine limit (for example, $\epsilon = 10^{-20}$).

Similar to those in [14,15], for any piece-wise interpolation function $R_i(x)$, it is easy to prove the following fact.

Proposition 1. *Inequality* $\mathrm{d}[R_i(x)]/\mathrm{d}x \geqslant 0$ *is always held within* $[x_{i-\frac{1}{2}}, x_{i+\frac{1}{2}}]$ *for* $f_{i-\frac{1}{2}} \leqslant \bar{f}_i \leqslant f_{i+\frac{1}{2}}$, *while* $\mathrm{d}[R_i(x)]/\mathrm{d}x \leqslant 0$ *is always held within* $[x_{i-\frac{1}{2}}, x_{i+\frac{1}{2}}]$ *for* $f_{i-\frac{1}{2}} \geqslant \bar{f}_i \geqslant f_{i+\frac{1}{2}}$.

Proposition 1 states that the rational function (9) does not change the convexity of the interpolated profile within each mesh cell. Inequality $(\bar{f}_i - f_{i+\frac{1}{2}})(f_{i-\frac{1}{2}} - \bar{f}_i) < 0$ implies the exceptional case where a peak or a valley is transported. The above conclusion does not apply in this case. However, our numerical results show that the scheme tends to flatten a sharp corner rather than produce numerical wiggles.

Fig. 2 shows the interpolated profiles for a triangular wave and a step jump by the rational function. The magnitude of the numerical oscillations is limited to the order of the small positive ϵ, which is negligible in practical applications.

3. The PRM scheme

We consider the advection transport equation in a conservation form as

$$\frac{\partial f}{\partial t} + \frac{\partial}{\partial x}(uf) = 0, \tag{14}$$

where t refers to the time, x the spatial coordinate, u the characteristic speed and f the transported quantity.

A Godunov scheme can be cast into the following flux form,

$$\frac{\partial \bar{f}_i}{\partial t} = -\frac{(uf)_{i+\frac{1}{2}} - (uf)_{i-\frac{1}{2}}}{\Delta x_i}. \tag{15}$$

Here $\bar{f}_i$ denotes the cell-integrated average of the transported quantity, while $(uf)_{i+\frac{1}{2}}$ and $(uf)_{i-\frac{1}{2}}$ the fluxes across the cell boundaries. The resulting numerical formulation is then automatically conservative.

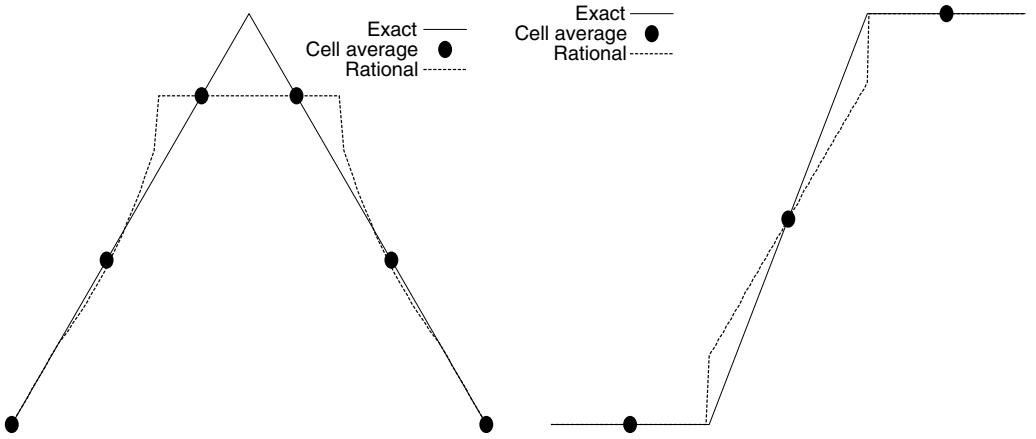

Fig. 2. Reconstruction for a triangle peak (left) and a step jump (right) by a rational function.

To get a high order scheme, the numerical flux is usually computed based on an interpolation which is more accurate than the piece-wisely constant approximation, e.g. the linear function in the MUSCL [11,12] and the parabolic function in the PPM [4].

Given the cell-integrated averages $\bar{f}_i^n$ at time step n, we first compute the cell interface values $f_{i+\frac{1}{2}}^n$ according to (3) for all mesh cells. The rational function (9) is then constructed in terms of $\bar{f}_i^n$, $f_{i-\frac{1}{2}}^n$ and $f_{i+\frac{1}{2}}^n$.

Remember that any interpolation function over $[x_{i-\frac{1}{2}}, x_{i+\frac{1}{2}}]$ can be expressed equivalently by two constructions based on either $x_{i-\frac{1}{2}}$ or, $x_{i+\frac{1}{2}}$ as

$$R_i^+(x) = \frac{a_i^+ + 2b_i^+(x - x_{i-\frac{1}{2}}) + \tilde{\beta}_i^+ b_i^+ (x - x_{i-\frac{1}{2}})^2}{[1 + \tilde{\beta}_i^+ (x - x_{i-\frac{1}{2}})]^2} \quad \text{for } x \in [x_{i-\frac{1}{2}}, x_{i+\frac{1}{2}}], \tag{16}$$

or

$$R_i^-(x) = \frac{a_i^- + 2b_i^-(x - x_{i+\frac{1}{2}}) + \tilde{\beta}_i^- b_i^- (x - x_{i+\frac{1}{2}})^2}{[1 + \tilde{\beta}_i^- (x - x_{i+\frac{1}{2}})]^2} \quad \text{for } x \in [x_{i-\frac{1}{2}}, x_{i+\frac{1}{2}}]. \tag{17}$$

For easier coding, we can choose R^+ or R^- according to the upwind direction. Let $\gamma_i^+ = 1 + \tilde{\beta}_i^+ \Delta x_i$, the coefficients of $R_i^+(x)$ can be immediately obtained as

$$a_i^+ = f_{i-\frac{1}{2}}^n, \tag{18}$$

$$b_i^+ = \frac{1}{\Delta x_i}(\gamma_i^+ \bar{f}_i^n - f_{i-\frac{1}{2}}^n), \tag{19}$$

$$\tilde{\beta}_i^+ = \Delta x_i^{-1} \left(\frac{|f_{i-\frac{1}{2}}^n - \bar{f}_i^n| + \epsilon}{|\bar{f}_i^n - f_{i+\frac{1}{2}}^n| + \epsilon} - 1 \right). \tag{20}$$

The coefficients of $R_i^-(x)$, denoted as $\tilde{\beta}_i^-$, γ_i^-, a_i^- and b_i^- can be found by just permuting $f_{i-\frac{1}{2}}^n$ and $f_{i+\frac{1}{2}}^n$ and replacing Δx_i with $-\Delta x_i$ in the corresponding expressions for $R_i^+(x)$.

After all the pieces of the interpolation function $R_i(x)$ are determined, the cell-integrated average $\bar{f}_i$ is updated by the flux formulation

$$\bar{f}_i^{n+1} = \bar{f}_i^n - (g_{i+\frac{1}{2}} - g_{i-\frac{1}{2}})/\Delta x_i, \tag{21}$$

where $g_{i+\frac{1}{2}}$ represents the flux of f across boundary $x = x_{i+\frac{1}{2}}$ during $t^{n+1} - t^n$ and is computed as

$$g_{i+\frac{1}{2}} = \int_{t^n}^{t^{n+1}} \{\min(0, u_{i+\frac{1}{2}}) R_{i+1}^+[x_{i+\frac{1}{2}} - u_{i+\frac{1}{2}}(t - t^n)] - \max(0, u_{i+\frac{1}{2}}) R_i^-[x_{i+\frac{1}{2}} - u_{i+\frac{1}{2}}(t - t^n)]\}\mathrm{d}t. \tag{22}$$

Using (16) or (17), we have

$$g_{i+\frac{1}{2}} = -\frac{a_{i+1}^+ \xi + b_{i+1}^+ \xi^2}{1 + \tilde{\beta}_{i+1}^+ \xi}, \quad \text{for } u_{i+\frac{1}{2}} < 0; \qquad \frac{a_i^- \xi + b_i^- \xi^2}{1 + \tilde{\beta}_i^- \xi}, \quad \text{for } u_{i+\frac{1}{2}} > 0, \tag{23}$$

where $\xi = \int_{t^n}^{t^{n+1}} u(t)_{i+\frac{1}{2}} \mathrm{d}t$.

From the convexity preserving property discussed in the above section, we have straightforwardly the following statement.

Proposition 2. *For the uniform advection velocity, the PRM scheme does not create any new extremum if the conditions of Proposition* 1 *are satisfied.*

The conditions of Proposition 1 is enforced in the scheme by modifying the $\bar{f}_i^n$ as,

$$\bar{f}_i^n = \max[\bar{f}_i^n, \min(f_{i-\frac{1}{2}}^n, f_{i+\frac{1}{2}}^n)] \quad \text{and} \quad \bar{f}_i^n = \min[\bar{f}_i^n, \max(f_{i-\frac{1}{2}}^n, f_{i+\frac{1}{2}}^n)] \tag{24}$$

before computing the interpolation function. It should be noted that above modification to $\bar{f}_i^n$ is only used for constructing the interpolation function (16) or (17). Thus, transport is still exactly conservative.

In PRM, once the cell interface value is determined, only (18)–(20), (23) and (24) need to be computed to get the flux. The adjustment of the interface value to enforce the monotonicity is not required here. The corresponding part in the PPM consists of (1.5), (1.10) and one of (1.12) in [4]. A direct comparison of computational efficiency between PRM and PPM can be carried out by counting the numerical operations of those parts where two schemes are different from each other. Table 1 shows the numbers of computer operations required in the corresponding parts in both schemes. It is easy to see that PRM requires less operation counts than PPM. However, we should also note that the operation of division is relatively heavier compared with other arithmetic operations, so a comparison in terms of CPU time is dependent on the hardware and compiler. The PRM should be faster on any architecture equipped with advanced division pipelines.

Table 1
Operation counts of the different parts of PRM and PPM

Operation	PRM	PPM
=, +, −, ×, ABS(x)	21	43
÷	2	0
MAX(x) or min(x)	4	0
IF logic	0	3
Total	27	46

The multi-dimensional computation of PRM scheme can be implemented as those applied to the PPM scheme [2,7]. We have adopted the dimensional splitting to extend the scheme to multi-dimensions. For a variable velocity field, the solution from a simple splitting can not be monotonic even the velocity field is multi-dimensionally divergence free. Extra modifications [3,6,7] are required to correct these splitting errors. The splitting correction suggested by Clappier [3] is used in our multi-dimensional calculations.

4. Numerical tests

In order to evaluate the numerical results in a quantitative way, we use an l_2 norm error E_{TOT} as defined in [10],

$$E_{\mathrm{TOT}} = \frac{1}{N}\sum_{i=1}^{N}(\bar{f}_i^n - f_i^{\mathrm{exact}})^2, \tag{25}$$

where N is the number of the sampled mesh cells.

It is easy to know that the total error can be further divided into the dissipation error and the dispersion error,

$$E_{\mathrm{TOT}} = E_{\mathrm{DISS}} + E_{\mathrm{DISP}}, \tag{26}$$

with

$$E_{\mathrm{DISS}} = [\sigma(\bar{f}^n) - \sigma(f^{\mathrm{exact}})]^2 + (\bar{\bar{f}}^n - \bar{f}^{\mathrm{exact}})^2$$

and

$$E_{\mathrm{DISP}} = 2(1-r)\sigma(\bar{f}^n)\sigma(f^{\mathrm{exact}})$$

being the dissipation error and the dispersion error respectively. In the above expressions, $\bar{\bar{f}}^n$ and $\sigma(\bar{f}^n)$ represent the mean and the standard deviation of $\bar{f}^n$ respectively, and r is the correlation coefficient between the values of $\bar{f}^n$ and f^{exact} on the mesh cells.

4.1. Comparison with PPM

We firstly examined the grid refinement convergence rate of the PRM scheme. Sine waves with wave lengths of $20\Delta x$ and $40\Delta x$ were computed. A constant velocity $u = 1.0$ was set throughout the computational domain. Fig. 3 displays the numerical results after 1000 steps with a Courant number 0.2. The results of the PPM scheme are also included for comparison. For the long wave, the PRM produces quite similar results to the PPM method. For the short wave, however, the PRM scheme gives better solution than PPM.

Numerical errors are calculated from the data sampled over 80 grid points and given in Table 2. In order to evaluate the accuracy and convergence rates of both schemes, we include the numerical results for a long wave of $80\Delta x$ as well. The PRM scheme produces less errors for all wave lengths compared to PPM. The convergence rates of PRM and PPM are shown in Table 3. Higher than 2nd order convergence rates are observed for both schemes.

The transport of a triangle wave given initially as

$$f^0(x) = \begin{cases} 1 - \frac{|x|}{0.15}, & |x| \leqslant 0.15, \\ 0, & \text{others} \end{cases} \tag{27}$$

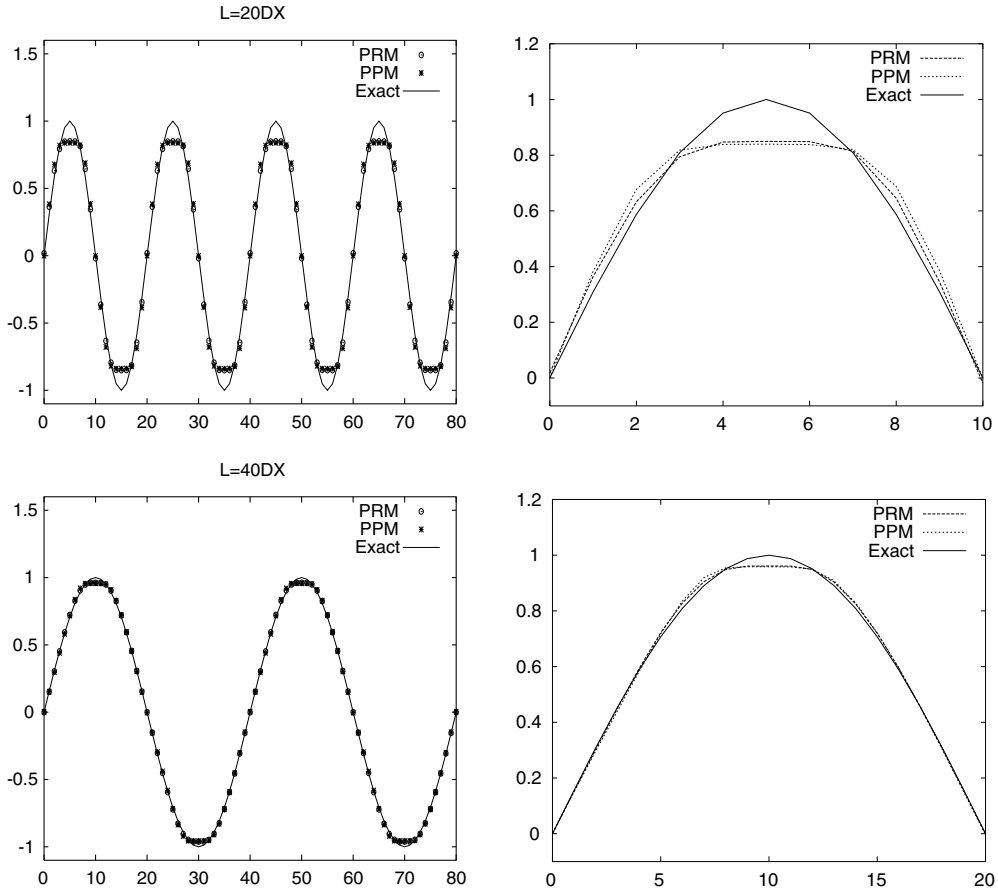

Fig. 3. Sine waves of the wave lengths being 20 (top) and 40 (bottom) grid-spacings transported after 1000 step calculations with the Courant number being 0.2. Displayed are the overall solutions (left) and the enlarged parts over half wave length (right).

Table 2
Grid refinement tests

Scheme	$E_{\mathrm{TOT}}(20\Delta x)$	$E_{\mathrm{TOT}}(40\Delta x)$	$E_{\mathrm{TOT}}(80\Delta x)$
PRM	5.36×10^{-3}	2.22×10^{-4}	7.06×10^{-6}
PPM	7.96×10^{-3}	3.22×10^{-4}	1.03×10^{-5}

Displayed are the errors defined by $E_{\mathrm{TOT}}=\frac{1}{N}\sum_{i=1}^{N}(\bar{f}_i^n-f_i^{\mathrm{exact}})^2$.

Table 3
Convergence rates of different schemes

Scheme	$\left[\frac{E_{\mathrm{TOT}}(20\Delta x)}{E_{\mathrm{TOT}}(40\Delta x)}\right]^{1/2}$	Order	$\left[\frac{E_{\mathrm{TOT}}(40\Delta x)}{E_{\mathrm{TOT}}(80\Delta x)}\right]^{1/2}$	Order
PRM	4.91	2.30	5.61	2.49
PPM	4.97	2.31	5.59	2.48

is computed to test numerical dispersion and shape preserving properties of the schemes. An equally spaced grid with $\Delta x = 0.01$ is used.

It is known that the numerical dispersion of high order schemes of flux form depends on the CFL number. We conducted numerical experiments for PRM and PPM with the CFL numbers of 0.02, 0.5 and 0.98. For the same transport distance, the number of steps are 10,000, 400 and 204 correspondingly. The numerical results of PPM and PRM are plotted in Fig. 4, and the deviations from the exact solution are shown in Fig. 5. When Courant number is 0.5, both schemes give spatially symmetric errors, thus there are not noticeable distortions to the symmetry of the initial profile. But for Courant number 0.02, PPM produces quite different errors for up-wind side and down-wind side of the triangle, and a significant distortion is observed on the down-wind side of the triangle from the results of PPM. The PRM, however,

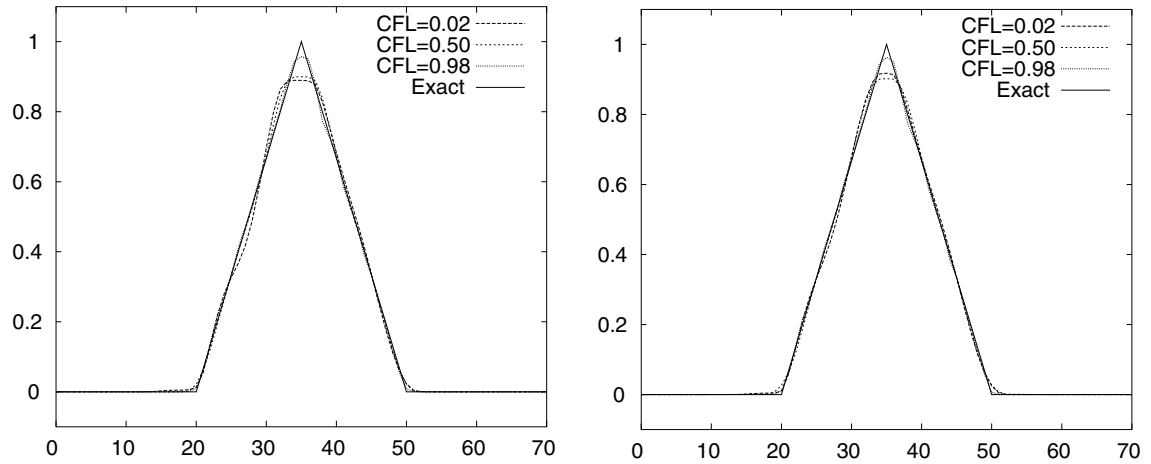

Fig. 4. A triangular wave transported by the PPM scheme (left) and PRM scheme (right) with the Courant number being 0.02, 0.5 and 0.98, respectively.

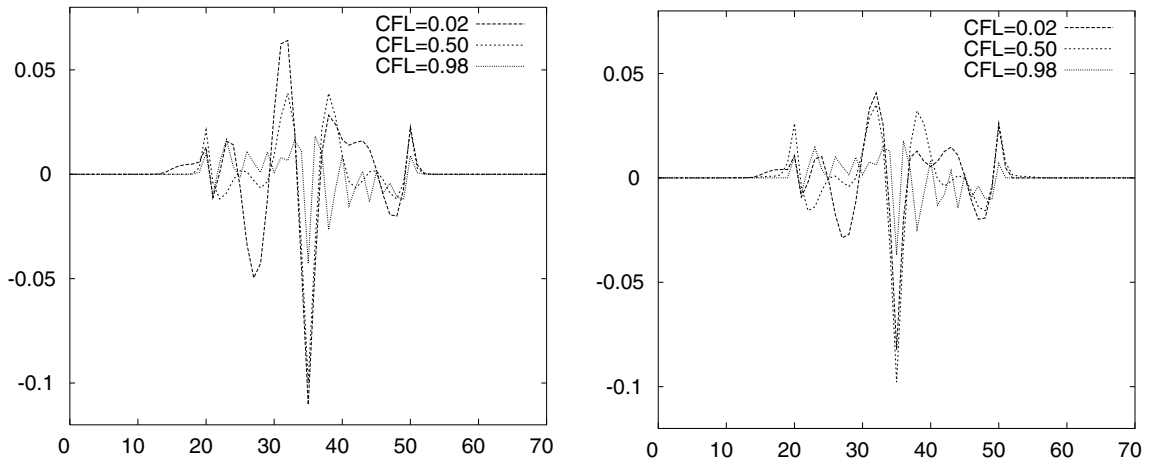

Fig. 5. The errors by $(\bar{f}_i^n - f_i^{\text{exact}})$ for the triangular wave transported by the PPM scheme (left) and PRM scheme (right) with Courant number being 0.02, 0.5 and 0.98, respectively.

Table 4
Numerical errors of a triangular linear wave computed by the PPM scheme

CFL no./steps	E_{TOT}	E_{DISS}	E_{DISS}/E_{TOT} (%)	E_{DISP}	E_{DISP}/E_{TOT} (%)
0.50/400	2.75×10^{-4}	1.01×10^{-6}	0.37	2.74×10^{-4}	99.63
0.02/10000	5.06×10^{-4}	1.05×10^{-6}	<0.01	5.06×10^{-4}	>99.99
0.98/204	7.44×10^{-5}	8.79×10^{-9}	<0.01	7.44×10^{-5}	>99.99

The data were sampled over 70 grid cells centered by the peak of the triangle with the CFL numbers being 0.5, 0.02 and 0.98, respectively.

Table 5
Same as Table 4, but computed by the PRM scheme

CFL no./steps	E_{TOT}	E_{DISS}	E_{DISS}/E_{TOT} (%)	E_{DISP}	E_{DISP}/E_{TOT} (%)
0.50/400	2.64×10^{-4}	1.90×10^{-6}	0.76	2.62×10^{-4}	99.24
0.02/10000	2.24×10^{-4}	7.36×10^{-7}	0.45	2.23×10^{-4}	99.55
0.98/204	6.17×10^{-5}	6.05×10^{-9}	<0.01	6.17×10^{-5}	>99.99

preserves the symmetry much better. Tables 4 and 5 show the numerical errors for different Courant numbers. In all cases the PRM scheme is more accurate than the PPM scheme in terms of the total numerical errors and the dispersion errors. PPM appears less accurate in dispersion as the Courant number departs from 0.5. It should be also noted that the PPM clips the triangular peak to a more significant extent, which is also observed in the sine wave tests.

To examine the capability of capturing discontinuities, the transport of a square wave is computed. The initial profile is defined as

$$f^0(x) = \begin{cases} 1, & |x| \leqslant 0.15, \\ 0, & \text{others.} \end{cases} \tag{28}$$

The computed results after 1000 steps with Courant number being 0.2 are plotted in Fig. 6. PRM produced almost the same numerical solution to the PPM and were able to bound the minimum values to

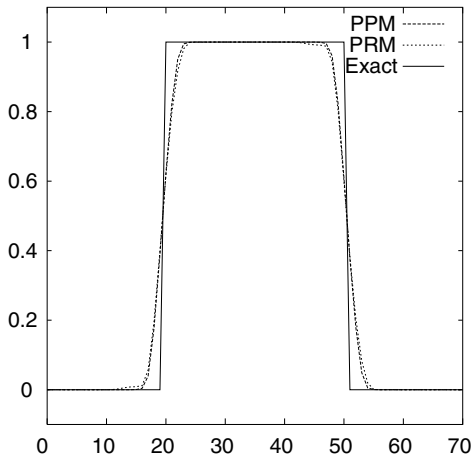

Fig. 6. Transport of a square wave with a constant velocity field.

Table 6
Square wave transportation problem

Scheme	RFM	RSM	MAX	MIN	E_{TOT}
PRM	1.0	0.937	1.0	$O(\epsilon)$	1.12×10^{-2}
PPM	1.0	0.944	1.0	0.0	1.02×10^{-2}

MAX and MIN indicate the highest and the lowest values produced by the schemes. Other quantities are defined as RFM $= \int \bar{f}(t) / \int \bar{f}(0)$ and RSM $= \int \bar{f}^2(t) / \int \bar{f}^2(0)$. The data are sampled over 70 mesh cells.

an order of ϵ, the small positive used in (20). The conservations in the total mass and the total squared mass, the maximum and the minimum of the numerical solutions, and the l_2 errors are shown in Table 6. The numerical manipulations to enforce the monotonicity in the PPM scheme always tends to clip a 'peak' to a 'plateau', and gives a better result to this particular test problem.

As the test of the 2D scheme, we solved the solid rotation test problems. The advection transport equation in 2D was computed on a $[0,1] \times [0,1]$ square with a 100×100 grid. A purely rotational velocity field with period 1 is specified as

$$u(x,y) = 2\pi\left(y - \frac{1}{2}\right), \quad v(x,y) = -2\pi\left(x - \frac{1}{2}\right).$$

Fig. 7 shows a cone after one revolution. The cone is initially centered at $(\frac{1}{2}, \frac{3}{4})$ with the base radius of 0.15 and the height of 1. The PRM gives a numerical solution competitive to the PPM with respect to shape preserving. Another test is conducted by using the initial profile of the cut-cylinder of Zalesak [17]. Shown in Fig. 8, the PRM again produced a numerical result among the best ones of this kind.

4.2. Smolarkiewicz's deformational advection test

We also repeated the test suggested in Smolarkiewicz [8] and Staniforth et al. [9] to transport a cone with a deformed flow field

$$u(x,y) = \frac{8\pi}{25} \sin\left(\frac{\pi x}{25}\right) \sin\left(\frac{\pi y}{25}\right), \tag{29}$$

$$v(x,y) = \frac{8\pi}{25} \cos\left(\frac{\pi x}{25}\right) \cos\left(\frac{\pi y}{25}\right). \tag{30}$$

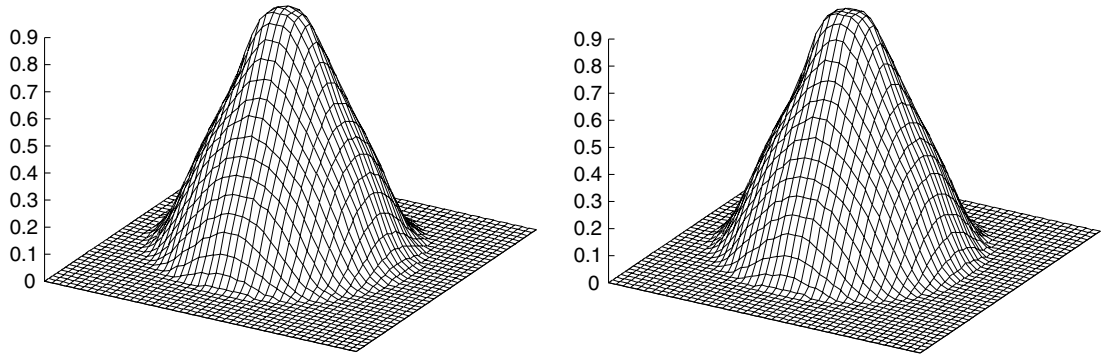

Fig. 7. Numerical solution after 1 revolution of the solid rotation test of a cone by PRM (left) and PPM (right).

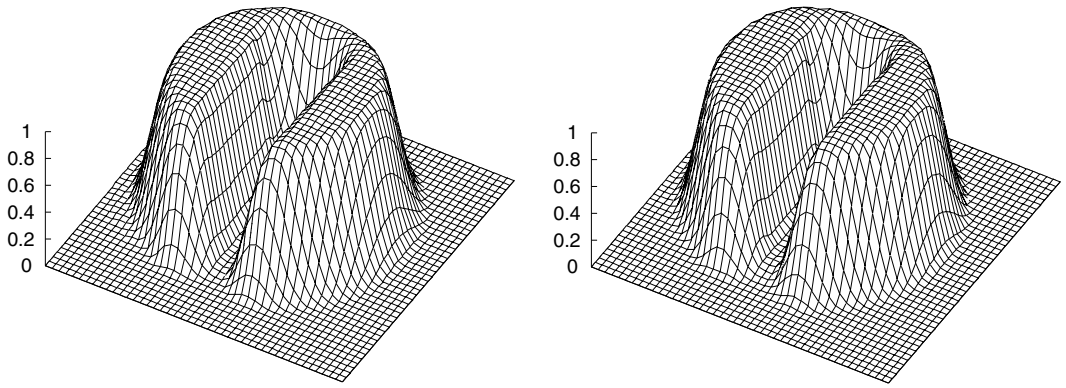

Fig. 8. Numerical solution after 1 revolution of the solid rotation test of a cut cylinder of Zalesak [17] by PRM (left) and PPM (right).

Corresponding to Bott [1], the numerical results at $T = 19\Delta t$, $38\Delta t$, $57\Delta t$ and $75\Delta t$ with $\Delta t = 0.7$ are plotted in Fig. 9. Our results agree with the analytical solution presented in Staniforth et al. [9] in terms of the overall shape and the phase of deformation. The symmetry of the solution is accurately reproduced.

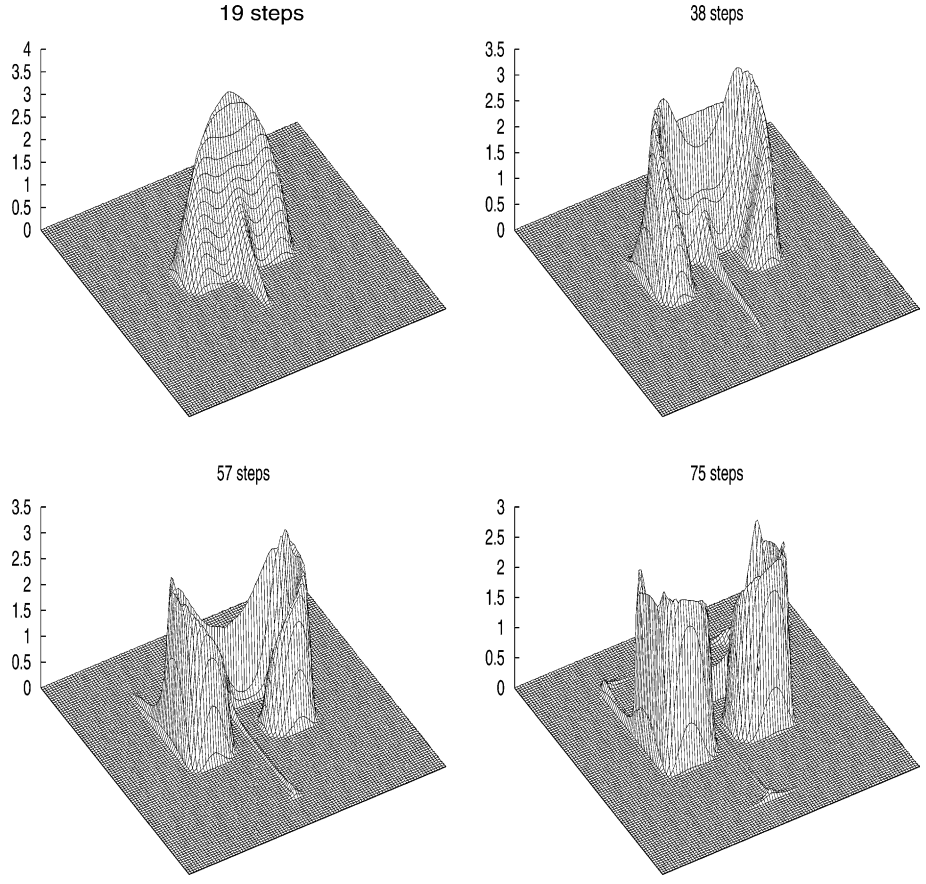

Fig. 9. Numerical results of the deformational flow field test for short time integrations computed by PRM.

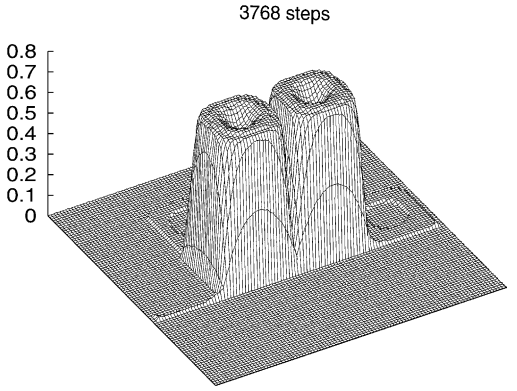

Fig. 10. Same as Fig. 9 but after 3768 steps.

However, same as any other stable scheme, PRM smeared the structures of thin film due to the finite resolution of computational mesh. Fig. 10 shows the computed result after 3768 steps with PRM scheme. As pointed out by Staniforth et al. [9] and Smolarkiewicz [8], the un-resolvable structure will develop as the time increases. But it is still meaningful to run a long time integration to see if the un-resolvable scales will cause computational instability for a scheme that works well with resolvable structures. The PRM has not encountered any computational instability even after a long integration time. The ratio of the second moment after 3768 steps to its initial value, $\sum(\bar{f}^2)_{3768\,\text{steps}}/\sum(\bar{f}^2)_{\text{initial}}$, is 0.299, which shows a dissipative property. The main feature that the concentration tends to move around the vortex centers after a long time integration was captured.

5. Conclusions

We have presented the PRM scheme as a conservative and oscillation-less advection scheme. The PRM is algorithmically simple and easy to code. Our numerical experiments show that the PRM is a competitive alternative to the PPM scheme with respect to numerical accuracy and computational efficiency. We can expect more applications of the PRM scheme to a wide range of CFD simulations.

Acknowledgements

We gratefully acknowledge the anonymous reviewers for their constructive comments on the original manuscript.

References

[1] A. Bott, A positive define advection scheme obtained by nonlinear renormalization of the advective fluxes, Mon. Wea. Rev. 117 (1988) 1006–1015.
[2] R.L. Carpenter Jr., K.K. Droegemeier, P.R. Woodward, C.E. Hane, Application of the piecewise parabolic method(PPM) to meteorological modeling, Mon. Wea. Rev. 118 (1990) 586–612.
[3] A. Clappier, A correction method for use in multidimensional time-splitting advection algorithms: application to two- and three-dimensional transport, Mon. Wea. Rev. 126 (1998) 223–242.

[4] P. Collela, P.R. Woodward, The piecewise parabolic method (PPM) for gas-dynamical simulations, J. Comput. Phys. 54 (1984) 174–201.
[5] S.K. Godunov, A difference scheme for numerical computation of discontinuous solutions of hydrodynamics equations, Math. Sbornik 47 (1959) 271–306 (in Russian).
[6] W. Hundsdorfer, E.J. Spee, An efficient horizontal advection scheme for modeling of global transport of constituents, Mon. Wea. Rev. 123 (1995) 3554–3564.
[7] S.J. Lin, R.B. Rood, Multidimensional flux-form semi-Lagrangian transportation schemes, Mon. Wea. Rev. 124 (1996) 2046–2070.
[8] P.K. Smolarkiewicz, The multi-dimensional Crowley advection scheme, Mon. Wea. Rev. 110 (1982) 1968–1983.
[9] A. Staniforth, J. Côté, J. Pudykiewicz, Comments on "Smolarkiewicz's deformational flow", Mon. Wea. Rev. 115 (1987) 894–900.
[10] L. Takacs, A two-step scheme for the advection equation with minimized dissipation and dispersion errors, Mon. Wea. Rev. 113 (1985) 1050–1065.
[11] B. van Leer, Toward the ultimate conservative difference scheme. Part IV: A new approach to numerical convection, J. Comput. Phys. 23 (1977) 276–299.
[12] B. van Leer, Toward the ultimate conservative difference scheme. Part V: A second order sequel to Godunov's method, J. Comput. Phys. 32 (1979) 101–136.
[13] F. Xiao, T. Yabe, Completely conservative and oscillation-less semi-Lagrangian schemes for advection transportation, J. Comput. Phys. 170 (2001) 498–522.
[14] F. Xiao, T. Yabe, T. Ito, Constructing oscillation preventing scheme for advection equation by rational function, Comput. Phys. Commun. 93 (1996) 1–12.
[15] F. Xiao, T. Yabe, X. Peng, H. Kobayashi, Conservative and oscillation-less atmospheric transport schemes based on rational functions, J. Geophys. Res. 107 (D22) (2002) 4609.
[16] T. Yabe, R. Tanaka, T. Nakamura, F. Xiao, Exactly conservative semi-Lagrangian scheme (CIP-CSL) in one dimension, Mon. Wea. Rev. 129 (2001) 332–344.
[17] S.T. Zalesak, Fully multidimensional flux corrected transport algorithm for fluids, J. Comput. Phys. 31 (1979) 335–362.